ELSEVIER

Nuclear Instruments and Methods in Physics Research A 433 (1999) 178–189

NUCLEAR INSTRUMENTS & METHODS IN PHYSICS RESEARCH Section A

www.elsevier.nl/locate/nima

Final tests of the CsI-based ring imaging detector for the ALICE experiment

for the ALICE collaboration

F. Piuz[a,*], A. Braem[a], M. Davenport[a], D. Di Bari[b], A. Di Mauro[b], D. Elia[b], B. Goret[a], P. Martinengo[a], E. Nappi[a,b], G. Paić[a,c], J.C. Santiard[a], S. Stucchi[a], G. Tomasicchio[b], T.D. Williams[a]

[a]*CERN, European Organization for Nuclear Research, 1211 Geneva 23, Switzerland*
[b]*INFN and Dipartimento Interateneo di Fisica dell'Universitá di Bari, Bari, Italy*
[c]*Ohio State University, Columbus, OH USA*

Abstract

We report on the final tests performed on a CsI-based RICH detector equipped with 2 C_6F_{14} radiator trays and 4 photocathodes, each of $64 \times 38\ cm^2$ area. The overall performance of the detector is described, using different gas mixtures, in view of optimizing the photoelectron yield and the pad occupancy. Test results under magnetic field up to 0.9 T, photocathode homogeneity and stability are presented.

1. Introduction and detector design optimization

In a series of three papers we report about the performance of a prototype of a Ring Imaging Cherenkov detector based on a caesium iodide (CsI) photoconverter, the CsI-RICH. The technical description of a large prototype is presented in Ref. [1], while the final test results and a study dedicated to Cherenkov angular resolution and simulation are described in the present paper and in Ref. [2], respectively.

The CsI-RICH detector was proposed to form the High-Momentum Particle Identification system (HMPID) of the ALICE experiment [3]. This system will be composed of seven modules of $1.3 \times 1.3\ m^2$ each, aiming to complement the particle identification of the ALICE detector barrel in the 2–5 GeV/c momentum range. According to present models describing lead–lead central collisions at LHC at 2.75 TeV/nucleon, a maximum density of about 100 particles per square metre is expected at the single arm HMPID system when it is located at 5 m from the interaction point. Following basic pioneering works [4], the development of large CsI photocathodes (PCs) was initiated by the CERN R&D project, RD-26 [5], started in 1993 and pursued in the ALICE and other HEP collaborations proposing PID systems based on CsI-RICH (HADES [6], see also Ref. [7] COMPASS-NA58 [8], see also Ref. [9]). These papers finalize the R&D phase at CERN. A more

* Corresponding author.
E-mail address: francois.piuz@cern.ch (F. Piuz)

0168-9002/99/$ - see front matter
PII: S0168-9002(99)00349-6

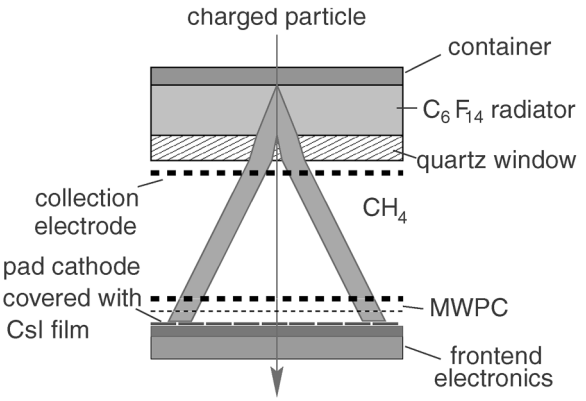

Fig. 1. Schematic cross-section of the CsI-RICH layout. The primary ionization deposited in the proximity gap is drained by the positively polarized wired electrode located close to the quartz window to avoid its collection by the photodetector. The main dimensions used in the large prototype are: radiator thickness: 10 mm, quartz window: 5 mm, MWPC gaps: 2 mm, wire cathode pitch: 2 mm, anode pitch: 4 mm, anode diameter: 20 μm, pad size: 8×8 mm^2.

detailed description of the development work and the detector elements is found in the ALICE/HMPID Technical Design Report [10].

Fig. 1 gives the main characteristics of the CsI-RICH layout. Cherenkov photons are emitted while charged particles traverse a 10 mm thick layer of C_6F_{14}. This liquid radiator medium is characterized by a refractive index and a low chromaticity which are adequate for particle identification in the momentum range required at ALICE. The Cherenkov photons impinge on the photodetector, separated from the radiator by a *proximity gap* of an adjustable depth, such that Cherenkov ring images of convenient size are obtained without a focusing device. The photodetector is an MWPC having its bottom cathode covered with a thin CsI layer, acting as a photoconverting plane. The same cathode is segmented into pads, of size 8×8 mm^2, in order to achieve a two-dimensional localization of the photoelectrons, mandatory in the ALICE high-density environment. Given the MWPC geometry, every single-electron event is detected as a pad cluster of typical size of 1–3 pads. The use of an analog multiplexed front-end (FE) electronics allows for a uniform low thresholding of 0.6 fC $\pm$ 0.03 [1,10] and accurate centroid localization.

The detector layout adopted for the CsI-RICH is quite attractive, because it allows a simple and economic design of large modules, composed of a radiator tray and a conventional MWPC, both enclosed in the same gas volume. However, the use of an MWPC with an open geometry and a two-dimensional pad readout necessitated careful optimizations in order to maintain a stable detector operation and to achieve the expected Cherenkov angular resolution in the high-density environment at ALICE. Hence, a crucial parameter is the fraction of pad hits per event, or pad occupancy, which has to be minimized in order to achieve the ring pattern recognition. Let us overview the two features expected to affect the pad occupancy and the chamber operation.

(i) As in any photoelectron detection based on the use of a wire chamber, the high gain, necessary for efficient single-electron detection, may lead to sustained discharges due to the photon feedback mechanism. The number N_{feed}, of secondary photons emitted isotropically by the primary avalanche is proportional to its size G, i.e. the chamber gain, and can be expressed as $N_{\mathrm{feed}} = k_1 \times G$, where k_1 is gas dependent. A fraction k_2 of these photons is converted by the photoconverting medium into secondary electrons and may initiate diverging processes if the product $k_2 \times N_{\mathrm{feed}}$ approaches 1.

(ii) The feedback generation of secondary electrons also results in enlarging the final cluster size, in case of overlap with the primary one, or even produces multi-cluster events, that increases the pad occupancy. The shape of the induced charge will be disturbed by such overlaps, degrading the centroid evaluation and the resulting localization accuracy.

Facing the necessity of minimizing the gas gain, the CsI-RICH layout has several beneficial features allowing to preserve the single-electron detection efficiency. Contrary to gaseous photoconverters, only a fraction of the feedback photons, isotropically emitted in the chamber gas, will be converted, thanks to the planar PC geometry. Indeed the wider the emission angle of the feedback photon, the more probably it will be lost by reflection on the dielectric surface of the CsI PC. Furthermore, since the pad size is large compared to the gap, the secondary conversions frequently occur at the same pad as the primary one, in fact reinforcing the induced signal.

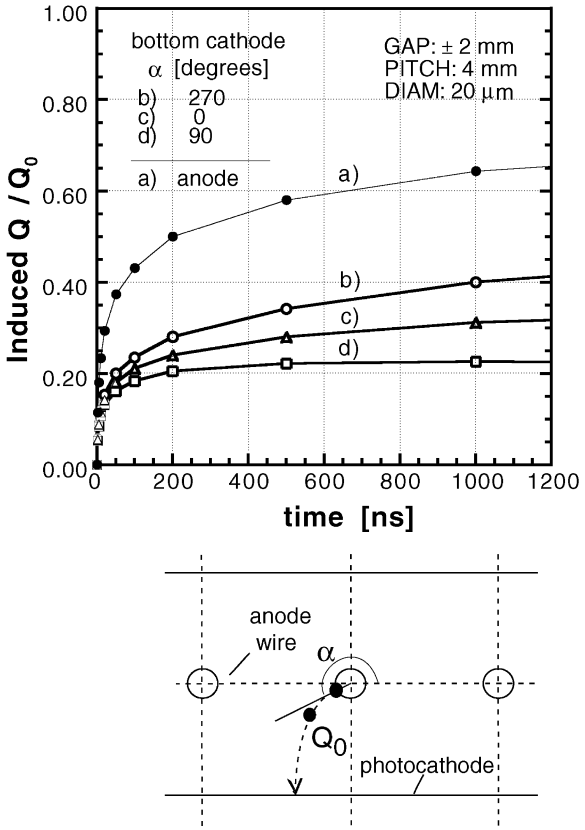

Fig. 2. Charge induced at the anode (a) and at the bottom cathode (b–d) by the motion of the ionic charge Q_0 as a function of time. At time 0, Q_0, the avalanche charge, is assumed punctual and located at the anode wire at a polar angle α defined in the drawing at the bottom. The 3 curves are plotted for 3 different starting angles, $\alpha = 0°$, $90°$ and $270°$. The induced charge is expressed as a fraction of Q_0 and represents the charge to be measured with a front-end electronics of integrating time T. In the CsI-RICH, the α values range from $180°$ to $360°$ since the photoelectron is emitted by the bottom cathode. The ion mobility is 1.5×10^{-6} cm^2/s^1 V^1.

The primary photoelectron, being emitted by the measuring pad, leads to an optimal an-ode-to-cathode coupling, since the avalanche always develops in the gap where the induced signal is measured, as shown in Fig. 2 [11].

2. Basic CsI-RICH study

Let us first introduce the experimental quantities used to evaluate the detector performance expressed by

$$N_{\mathrm{phel}} = LN_0\varepsilon_{\mathrm{det}} \sin^2 \theta_{\mathrm{c}} \quad (1)$$

where N_{phel} is the number of Cherenkov photoelectrons, L is the radiator thickness, θ_{c} is the Cherenkov angle, $\varepsilon_{\mathrm{det}}$ is the single-electron detection efficiency and N_0 is the detector factor of merit [12].

As seen in Fig. 3, the pad array is divided into three zones: a zone surrounding the particle impact, a Cherenkov ring fiducial zone, and the rest of the pattern corresponding to background hits. They are referred to as MIP, fiducial, and background zones, respectively. The variables listed below can be independently analysed for each zone of the pad array:

(a) N_{pad}: the total number of hit pads per zone.
(b) N_{raw}: the number of raw clusters per zone; a raw cluster is defined as a pad pattern having all pads adjacent by at least one edge. Large-sized clusters are usually formed by several overlapping single patterns.
(c) N_{res}: the number of resolved clusters per zone; in the fiducial zone a resolved cluster is assumed to correspond to a single Cherenkov

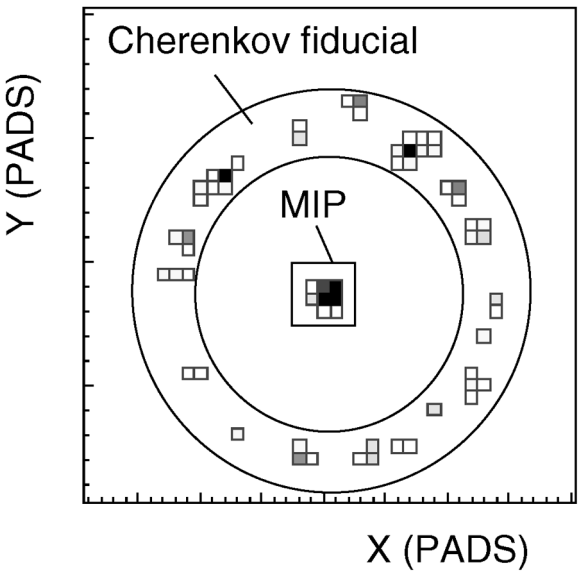

Fig. 3. Single Cherenkov ring event with the three zones used for cluster finding. A pad unit is 8×8 mm^2.

photoelectron according to deconvolution algorithms applied to raw clusters.

(d) N_{tot}: total number of single electrons (Cherenkov and photon feedback) inside a fiducial Cherenkov area.

(e) A_0 is the mean of the single-electron pulse-height distribution (SE-PHD) seen in the next figure, obtained from resolved clusters. In what follows, A_0 will be the variable used to study the detector properties as function of the chamber gain, in order to normalize all results to the chamber gain independent of the experimental conditions (different gas pressure, gas mixtures, gap, etc.). The chamber gain is proportional to A_0 with a factor given by Fig. 2 at our working integration time of 700 ns. A_0 is expressed in units of ADC-channel, one unit being equivalent to 0.17 fC or 1062 electrons in our experimental setup [1,10]. Note that the ratio of the total pad pulse height (PH) measured inside the ring fiducial zone over A_0 provides N_{tot} whatever the cluster overlaps are.

2.1. Experimental setup

Several CsI-RICH prototypes were built and tested: Proto-1 has $32 \times 30\ cm^2$ active area; Proto-2 has $0.8 \times 1.3\ m^2$ active area and comprises 4 CsI

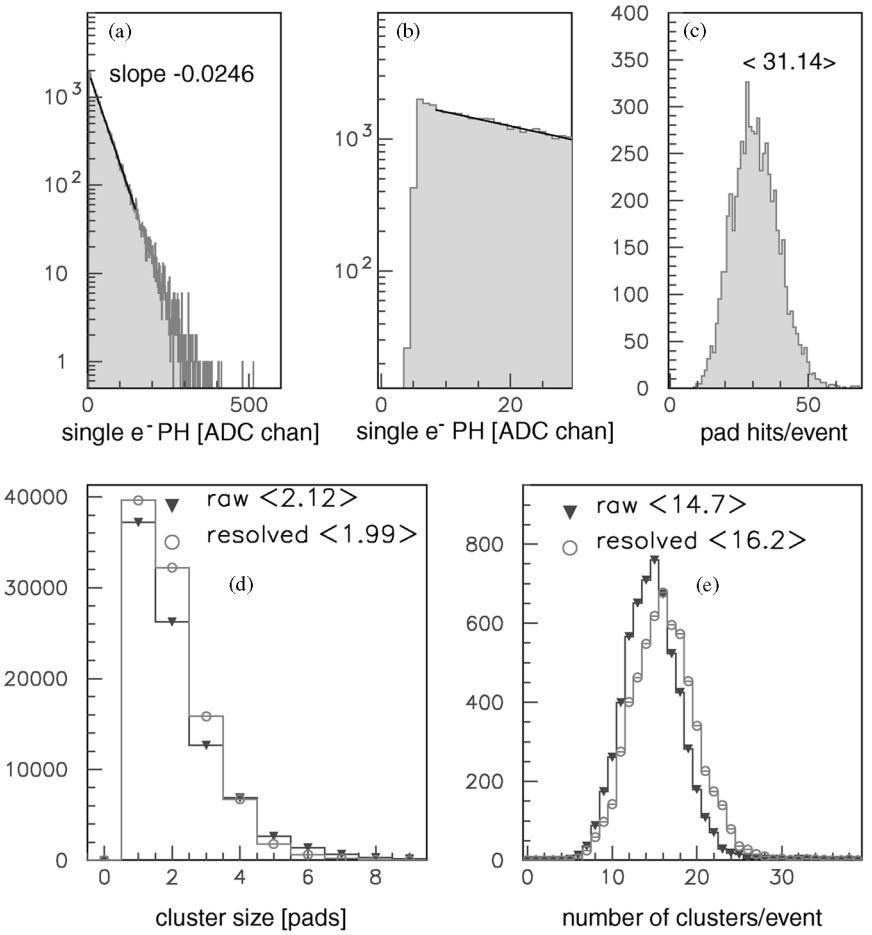

Fig. 4. Experimental distributions from the SPS beam test: 350 GeV/c pion at normal incidence, radiator: 10 mm C_6F_{14}, detector gas: CH_4, anode voltage: 2100 V. (a) Single-electron PH spectrum, (b) the lower part of spectrum (a) with the PH threshold in evidence (one ADC channel corresponds to 0.17 fC), (c) number of pad hits per ring, (d) size and (e) frequency of raw and resolved clusters in the fiducial zone.

PCs of $64 \times 38\,cm^2$ and 2 radiator trays, $133 \times 40 \times 1\,cm^3$ each, filled with C_6F_{14}. This prototype is exactly $\frac{2}{3}$ of a full size HMPID module in ALICE.

The detectors were tested at the CERN-PS/T11 beam line using positive secondary particles of 1–3.5 GeV/c and at the CERN/SPS-H4 line using 350 GeV/c pion beam, allowing also for exposure to dense multi-particles events obtained by interactions on target. The test setup was usually a telescope composed of a trigger system, a set of 4 tracking pad chambers and a time-of-flight array [10].

2.2. Characteristic experimental distributions and dependence on the chamber gain

Fig. 4 shows some distributions characterizing a test run of Proto-2 at the SPS. In particular, plot (b) gives a zoom-in at low PH values of the SE-PHD shown in (a), the steep edge of the distribution represents the mean threshold value achieved by the FE electronics [1,10]. This value, A_{th}, of 3–4 ADC channels, corresponds to 3–4 times the sigma of the electronic noise distribution measured for every channel. The single-electron efficiency, ε_{det}, is represented in Fig. 5 as a function of the single-electron mean PH, according to $\varepsilon_{det} = \exp(-A_{th}/A_0)$ applicable in the case of exponential SE-PHDs.

Fig. 6 shows characteristic plots derived from the previous distributions as function of the mean PH. One can notice (6a) that N_{res} tends to reach a plateau of 15–16 Cherenkov photoelectrons per ring, while the total number of electrons N_{tot} increases almost linearly with the chamber gain. Such a linear dependence is expected since the feedback photons add a contribution that increases linearly with the chamber gain (Eq. (1)). On the contrary, N_{res} remains flat, as expected at the full detection efficiency plateau and since primary and secondary clusters frequently overlap for geometrical reasons. As pointed before, such a feature has a beneficial effect on the detection efficiency since a fraction of the events is composed of two photoelectrons but, on the other hand, the feedback photons contribute also to increase the pad pattern occupancy by enlarging the size of the clusters and their number. This is illustrated in Fig. 6a showing N_{pad}, the number of pad hits per ring, monotonically increasing with the chamber gain. Fig. 6b shows the ratio of the total number of electrons to the number of Cherenkov resolved clusters, providing the mean number of photoelectrons per cluster. This number gives an approximate evaluation of the fraction of feedback photons, however, convoluted with a small contribution of primary Cherenkov clusters geometrically overlapped (Fig. 3). The rise of N_{tot}/N_{res} observed in Fig. 6b at low amplification results from the selection by thresholding of large-sized avalanches which may be originated by more than one photoelectron. In the next section, we shall investigate the possibility of reducing N_{tot}/N_{res}, i.e. the pad occupancy, by using different gas mixtures.

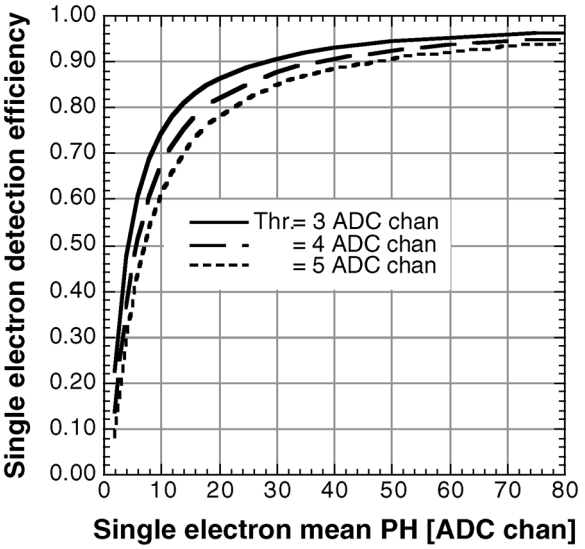

Fig. 5. Single-electron detection efficiency as function of the single-electron mean PH calculated at different experimental FE electronics thresholds. One ADC channel corresponds to 0.17 fC.

3. Other properties of the CsI-RICH

3.1. Influence of gas mixtures on photoelectron yield and photon feedback

It has been demonstrated in Refs. [13,14] that the operation of a CsI PC in a gas medium at

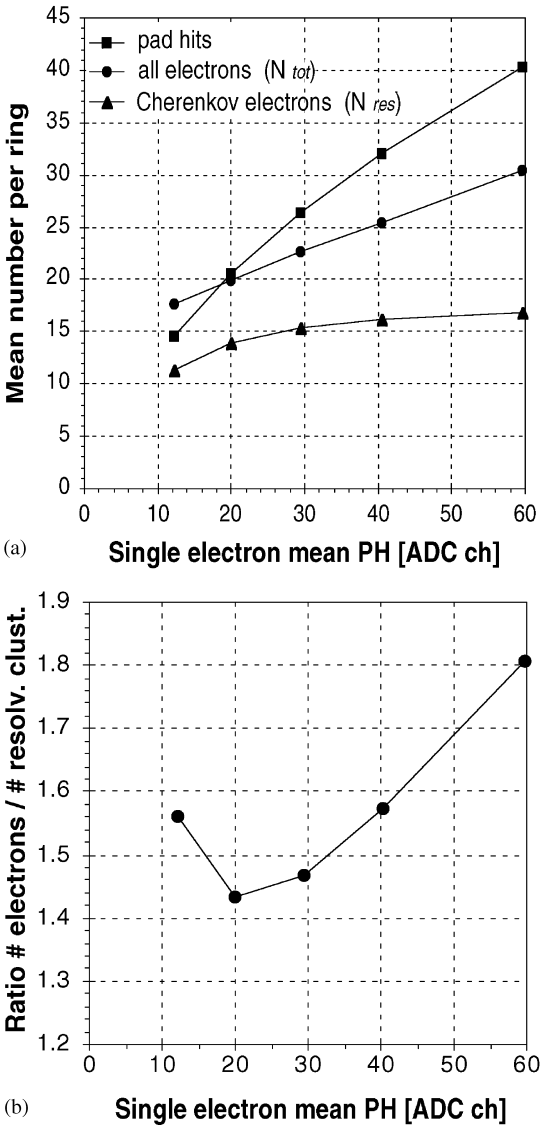

Fig. 6. (a) The mean number of pad hits (N_{pad}), the total number of electrons (N_{tot}) and the number of 'Cherenkov electrons' (N_{res}) per ring as function of the single-electron mean PH, obtained by varying the anode voltage. (b) Ratio N_{tot}/N_{res}, representing the mean number of electrons per clusters. One ADC channel corresponds to 0.17 fC. Experimental conditions: 350 GeV/c pions at normal incidence, radiator: 10 mm C_6F_{14}, detector gas: CH_4.

atmospheric pressure results in a loss of photoelectrons, depending on the gas species and the reduced field E/p value at the PC surface. Pure CH_4 was shown to cause only a few % loss, while noble-gas based mixtures considerably decrease the photoelectron yield. In addition, CH_4 has excellent UV transparency which is quite attractive. However, this good transparency makes its contribution to photon feedback non-negligible, due to the three emission lines at 156, 166, 193 nm. In addition, recent results from GALICE simulation show how important the conversion of slow neutrons in a hydrogenated gas could be. These very heavily ionizing events ($\sim$ MeV local energy deposition) might be responsible for damaging the chamber. We present a study of the influence of the gas mixtures on the photoelectron yield and the photon feedback ratio.

In Fig. 7, N_{res} and the ratio N_{tot}/N_{res} are plotted as a function of A_0, for various gas mixtures, CH_4,

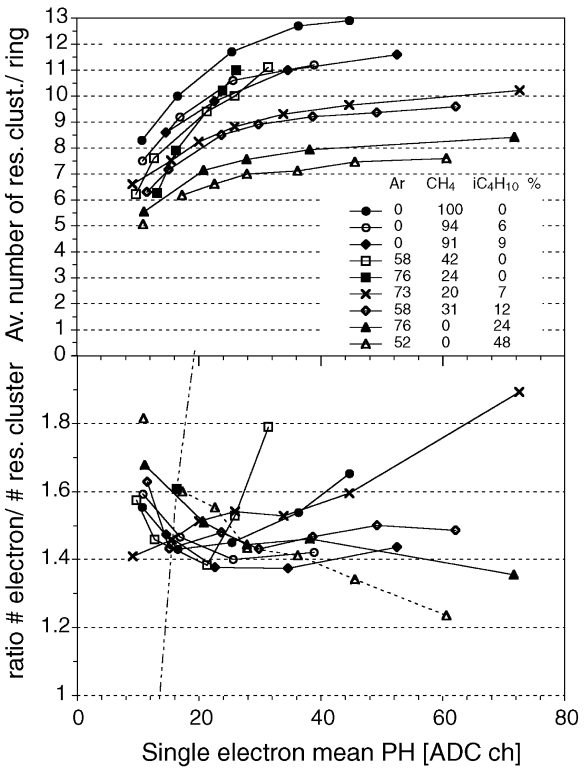

Fig. 7. Gas mixtures studies: Proto-1, 350 GeV/c pions at normal incidence, radiator: 10 mm C_6F_{14}. (a) The mean number of Cherenkov electrons per ring (N_{res}) as a function of the single-electron mean PH. (b) The ratio N_{tot}/N_{res}, representing the mean number of electrons per cluster. One ADC channel corresponds to 0.17 fC.

CH_4/i-C_4H_{10}, Ar/CH_4, Ar/i-C_4H_{10}, Ar/CH_4/i-C_4H_{10}. i-C_4H_{10} is known for its efficient quenching property.

Fig. 7a shows that the photoelectron yield is maximum using pure CH_4, and decreases when increasing the i-C_4H_{10} fraction in the mixture. Compared to pure CH_4, the photoelectron yield loss is 13% by adding 10% i-C_4H_{10} and 45% in Ar/i-C_4H_{10} (52/48). A part of that loss can be attributed to a poorer i-C_4H_{10} UV transparency (the 98.7% purity i-C_4H_{10} used in our test was not purified by Oxysorb cartridges). The 'noble-gas backscattering effect' [13,14] can be evaluated by comparing mixtures having about the same i-C_4H_{10} fraction, that is CH_4/i-C_4H_{10} (94/6) and Ar/CH_4/i-C_4H_{10} (73/20/7) where the loss is 20%. Ar/CH_4 mixtures seem able to achieve the same plateau as CH_4; however, owing to the poor quenching of CH_4, the feedback yield is so high that the cluster resolution is degraded. In addition, microdischarges were observed at such a rate that the use of these mixtures is out of question for stable operation.

Fig. 7b shows the variation of the ratios N_{tot}/N_{res} as a function of A_0. As said above, N_{tot}/N_{res} quantifies the fraction of photon feedback per ring in the Cherenkov fiducial zone. A rapid increase of the photon feedback yield is observed in Ar/CH_4 mixtures already at low gain, making these mixtures useless even with 50% CH_4. For the other mixtures, N_{tot}/N_{res} shows a minimum at ADC channel 20–30. In fact the falling part on the left of the plots comes from the poor efficiency at low A_0, as seen in Fig. 7a. The lowest minimum value, 1.38, is obtained with CH_4/i-C_4H_{10} mixtures for A_0 up to 40 ADC channels, providing full single-electron detection efficiency (Fig. 5). Although a comparable minimum is achieved in pure CH_4, it is obtained at lower A_0, with only about 60% efficiency. Ternary and Ar/i-C_4H_{10} mixtures show a ratio almost constant with A_0 but, as seen in Fig. 7a, the photoelectron yield might be too low.

In conclusion, the best mixture from the point of view of detector performance seems to be CH_4/i-C_4H_{10}, allowing to reach the smallest pad occupancy at the cost of a slightly reduced N_{res} value. However, the large hydrogen content increases the neutron conversion. Another candidate, containing less hydrogen, could be Ar/CH_4/i-C_4H_{10} 58/31/12.

3.2. Minimum Ionizing Particle (*MIP*) detection and associated background

In order to study the pad patterns specific to MIPs, in the absence of Cherenkov events, measurements were taken after emptying the radiator. The beam spot size at the chamber was of a few tens of mm^2 (pion, 350 GeV/c).

Given the high yield of feedback photons associated with large MIP avalanches, an MIP event can contain several separated clusters. Fig. 8a shows the total number of clusters per event, which can be split into two groups. A small fraction comes from secondary interactions that are identified by the external pad chamber telescope. The larger group of clusters is identified as the feedback photon contribution, since their PH distribution is found exponential and comparable to that of single Cherenkov photoelectrons under the same detector gain [10]. In Fig. 8b, the mean cluster size is plotted versus the chamber gain only for single clustered MIP events (primary and secondary clusters are overlapping). The distance of the clusters (only those found outside the MIP primary cluster area) from the MIP impact is plotted in Fig. 8c. This distribution extends to large distances not compatible with the assumption that the emitting secondary photon source is located at the anode wire only. One has to assume emitting sources more distant from the pad plane like parasitic Cherenkov light (delta rays in the quartz window) or reflections at the quartz surfaces.

In conclusion, feedback photons increase the pad occupancy of MIP events by generating on the average about 2 clusters per MIP. The centroid accuracy is also slightly affected by cluster overlaps.

3.3. Influence of magnetic field on the photoelectron yield

When operating the CsI-RICH in a magnetic field parallel to the PC plane, photoelectrons, emitted nearly at rest from the CsI PC, are submitted to the resulting force of crossed electrical and magnetic fields. Depending on the energy and emission

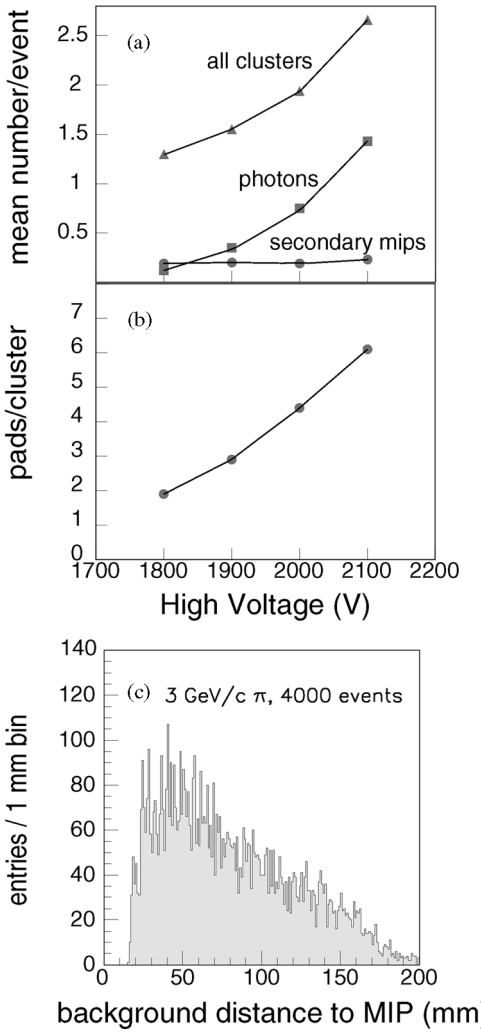

Fig. 8. MIP detection with empty radiator, 350 GeV/c pions at normal incidence, detector gas: CH_4. (a) Background associated to MIP primary clusters: number of clusters per event as function of HV. (b) Mean size of single cluster events as function of HV. (c) Distribution of the distance of background secondary clusters to the impact point of their primary MIP.

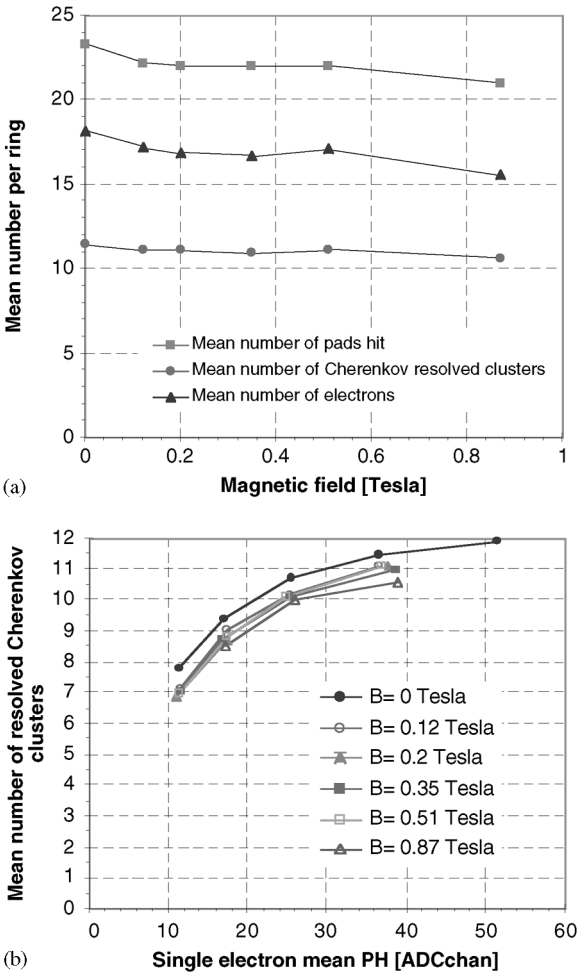

Fig. 9. (a) The performance of a CsI PC placed parallel to a uniform magnetic field. (b) Mean number of Cherenkov electrons per ring (N_{res}) as a function of the chamber gain at different magnetic field intensities. Part of the drop with respect to no-field value originates from an increase of the common noise induced by the magnet operation. Experimental conditions: Proto-1, 350 GeV/c pions at normal incidence, radiator: 10 mm C_6F_{14}. One ADC channel corresponds to 0.17 fC.

angle of the photoelectron, the curling of its trajectory during the first mean free path in the gas could send it back to the PC. Since, to our knowledge, the distributions of the energy and emission angle of the photoelectron are not available, a direct test was carried out installing proto-1 inside the GOLIATH magnet of NA57, providing an adjustable field between 0 and 1.5 T, parallel to the PC. We used pions of 350 GeV/c. Fig. 9a shows the variations of N_{pad}, N_{res} and N_{tot} as a function of the magnetic field measurements taken at the same gas gain: a slight decrease is observed of about 8% at 0.9 T. Fig. 9b shows the variations of N_{res} versus A_0, which is proportional to the electrical field at

the PC surface, for various magnetic field values. It can be seen that the curves remain parallel at different magnetic fields down to the minimum electrical field. The E/p under test range from 3.8 to 4.2 (V/cm)/Torr. In conclusion, the operating magnetic field at ALICE of 0.2 T is not expected to affect the performance of the CsI-RICH.

4. Long-term performance of the CsI-RICH prototypes

4.1. Operation of the detector, chamber current

Despite the presence of a semi-insulating CsI layer, the commissioning of a new PC has never required any conditioning time: the working voltage is reached in less than one hour with a very low dark current (less than 10 nA) and very rare 'micro-discharge' events when CH_4 or CH_4/i-C_4H_{10} mixtures are used. The noble-gas based mixtures are more unstable under local beam irradiation at 10^4 1/cm^2 s rate, where voltage trips are observed. The dark current delivered by the 1 m^2 area of the large prototype is 1–2 nA and is stable during beam operation. Local beam irradiation up to 2×10^4 1/cm^2 s can be sustained. Such a rate is several orders of magnitude larger than the local rate expected at ALICE (10–50 particles/cm^2 s).

4.2. Photon yield uniformity

In order to evaluate the uniformity of the photoelectron yield of a CsI PC, pad patterns of rings are overlapped to create a two-dimensional hit density plot that allows in turn to plot the hit density per unit angle versus azimuthal angle of the ring. Such a plot is shown in Fig. 10, indicating a uniform response all around the ring. The variation of the azimuthal density was never found to be larger than 10%, demonstrating a satisfactory uniformity of the response of the PC over its whole area.

4.3. Stability of the CsI photocathode

Following a first performance evaluation just after production, several PCs were periodically re-evaluated at the test beam in order to control their stability versus chemical contaminations such as moisture, oxygen, etc. Fig. 11a shows the evolution of PC19 and PC24, two of our oldest PCs. Even though these PCs were removed and remounted about 10 times from proto-1, under non optimal conditions, long plateaus are observed corresponding to less than 5% QE drop over three years. The production and the handling of the last PCs, PC29–PC32, equipping the large prototype, were performed with more care and better controls. They show, in Fig. 11b, an excellent stability over their first year of operation.

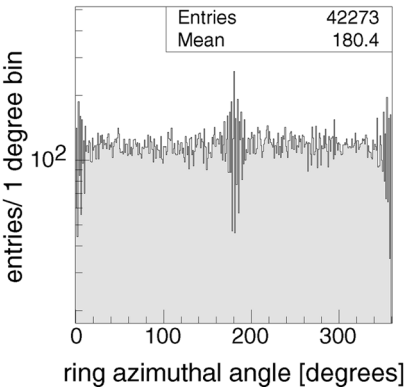

Fig. 10. Azimuthal distribution of the number of hits in a 1° bin along the Cherenkov fiducial zone. (3000 events, PC32, radiator: 10 mm C_6F_{14}, detector gas: CH_4, anode voltage: 2050 V).

5. Final beam test of CsI-RICH prototype

The large prototype was assembled in 1996 and the first large PC, PC26, tested at PS/T11 in December 1996. The four final PCs (PC29–PC32) were processed and tested with small radiators at T11 from June to October 1997, followed by three periods at the SPS-H4 line, ending in July 1998. Single-particle runs were taken scanning at three beam positions the four PCs, at different particle incident angles: 0–10° by step of 2.5°. It is shown in Fig. 12 that the number of Cherenkov photons per ring, N_{res}, is slightly decreasing when the track incident angle increases from 0° to 10°.

The total time of exposure to the beam was about 30 days. The irradiation rate was typically

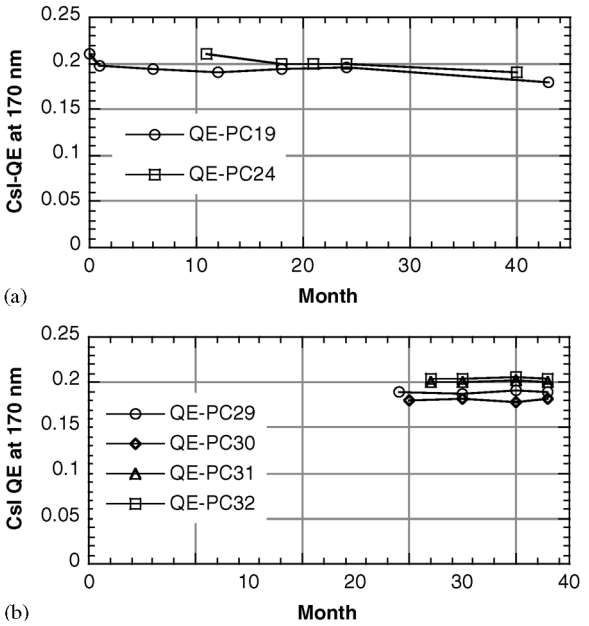

Fig. 11. Evolution of the CsI PCs quantum efficiency, evaluated in beam tests as described in Ref. [12], from the deposition time. (a) PC size: 30×30 cm^2. (b) PCs of 64×38 cm^2 size equipping the large prototype, PC29 to PC32. When not exposed to the test beam, the PCs are continuously flushed with argon at 30 l/h.

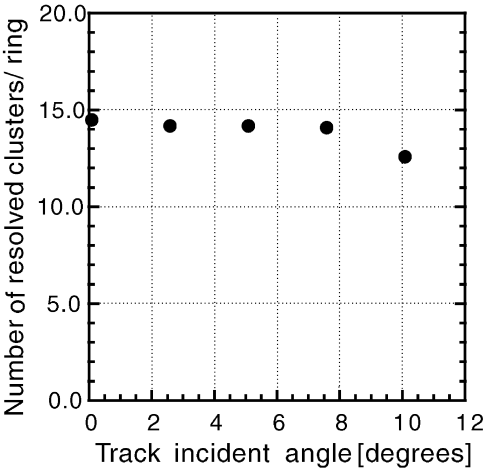

Fig. 12. Mean number of Cherenkov electrons per ring (N_{res}) as a function of the incident angle of the MIP track. Experimental conditions: 350 GeV/c pions, radiator: 10 mm C_6F_{14}, detector gas: CH_4, anode voltage: 2100 V.

5 kHz on a beam spot of 1 cm^2, corresponding to a maximum current of 30 nA/cm^2 at maximum gain. During monitoring, neither microdischarges nor HV trips were observed, indicating a quite stable operation. CH_4 was mainly used as amplification gas at a flow of 30 l/h. The contamination level was kept at less than 10 ppm for oxygen and moisture. The description and performance of the C_6F_{14} radiator system are reported in Ref. [10].

In Fig. 13a, the variation of the gain A_0 is represented versus the chamber voltage obtained with the beam centred at the middle of each PC. While the same gain curves are measured in the quadrants of the chamber corresponding to PC30 and PC32, the curves are shifted by $+30$ V for PC31 and -30 V for PC29, with respect to PC30, PC32. At an operational voltage of 2050 V, that shift corresponds to a 20% variation of the chamber gain. Given the relative positions of PC29 and PC31 on the detector, the gap variation cannot be attributed to an overall deformation of the main frame due to the overpressure but to gap differences of each pad panel resulting from the adjustment procedure (frame machining). Such a gain difference corresponds to a variation of 120 μm of the nominal 2 mm gap value. The incidence on the clustering is shown below.

In Fig. 13b, the photoelectron yield, N_{res}, and the number of pads hit per ring in the four PCs are compared. A mean value of $N_{res} = 14.9 \pm 1.5$ is obtained at $A_0 = 40$ ADC channels. This spread is not correlated to the different gains reported in Fig. 13a: PC31 and PC32, achieving the best yields, are located in gaps of low gain. This reflects, in fact, a spread in the QE value, as seen in the plot (c) of the ratio N_{tot}/N_{res} correlating PCs of low QE to PCs of low photon feedback. This spread is actually found acceptable in the context of our pattern recognition efficiency. The prototype was operated in July 1998 with CH_4/i-C_4H_{10} mixtures. When adding isobutane, the photoelectron yield drops down by 10–20% accompanied by a significant decrease of the feedback photon yield at high gain.

Finally, the prototype was exposed to multiparticle events at SPS/H4, obtained by the 350 GeV/c pion beam interacting on a beryllium target. A telescope composed of four pad chambers was used for the full event reconstruction. Still, the detector

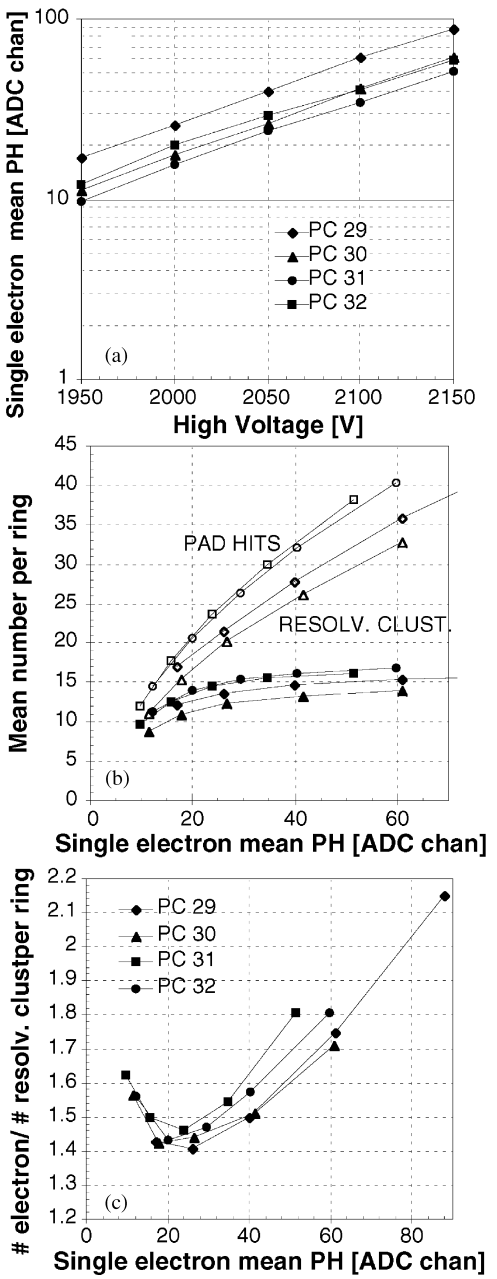

Fig. 13. A comparison of the performance of the 4 PCs (PC29 – PC32) mounted inside the large prototype. Experimental conditions: 350 GeV/c pions at normal incidence, radiator: 10 mm C_6F_{14}, detector gas: CH_4. (a) Single electron mean PH as a function of HV, measured at the centre of each PC. As function of the single electron mean PH: (b) mean N_{res} and N_{pad} per ring, (c) the ratio N_{tot}/N_{res} (feedback photon fraction). One ADC channel corresponds to 0.17 fC.

showed stable operation, though submitted to heavily ionizing events and local secondary track density of up to 100 per m^2 [10].

5.1. Ageing and 'heavily-ionizing' events

In addition to the degradation provoked by contaminants, a CsI PC operated in an MWPC may be damaged by the impact of the ions cloud of each avalanche. Taking the ion charge per photoelectron and MIP as 8×10^{-14} and 1.2×10^{-12}C, respectively, at a maximum gain of 5×10^5, the beam rates routinely used at the test beams were equivalent to 3×10^{-8}(C/cm^2)/s. Thus the charge density integrated over a 1 year lead run at ALICE (corresponding to 10^6 s), amounting to 0.05 mC/cm^2, was largely overcome during the test exposure without showing any degradation of the PCs.

In 1995–1996, a relevant information was obtained from the operation, during two periods of four weeks each, of a CsI-based imaging detector built in our group for the NA44 experiment, using lead beam on target. The CsI photodetectors, part of the Threshold Imaging Cherenkov detector (TIC [15,16]) were located close to the lead beam dump and were delivering high burst current (100–400 nA). However, the magnetic spectrometer in use at NA44 was designed such that very few charged particles were traversing the gaseous radiator of the TIC without even crossing the photodetectors. Hence, it is expected that a large part of the current was produced by neutrons. During these beam periods, the performance has been found stable and the detector operation was satisfactory.

In conclusion, although the ageing of CsI PCs at the present is neither well quantified nor fully understood, our detector has been found stable under ion rates much larger than those expected during the ALICE operation.

6. Conclusions

A 1 m^2 prototype of a CsI-RICH has been thoroughly tested under single and multi-particles irradiations. Equipped with a 10 mm thick C_6F_{14} radiator and four CsI PCs, each of 64×38 cm^2

area, a very stable operation has been demonstrated, achieving a single-electron detection efficiency larger than 90% at beam rates up to 20 kHz/cm^2. Following an extensive study of different gas mixtures, it has been shown that CH_4 or CH_4/i-C_4H_{10} provides the best photoelectron yield, 15–16 Cherenkov photons per ring. Despite the photon feedback, the pad occupancy could be kept low enough to allow for ring pattern reconstruction with a particle density of up to 50 particle per square metre [10]. It has been checked that the detector performance is not affected by a magnetic field, parallel to the PC plane, of up to 0.9 T. The stability of CsI layers has been demonstrated over a 44 months period. Based on these results, the CERN LHC committee has given its approval for the construction of the HMPID system at ALICE, that will consist of seven CsI-RICH modules of 2 m^2 area each.

Acknowledgements

After the completion of the R&D phase, the HMPID team (Bari and CERN groups) has the pleasure to acknowledge many colleagues, whose help was essential for the success of this work: A. Breskin, R. Chechik, C. Coluzza, A. Morsch, J. Séguinot, T. Ypsilantis and our RD-26 colleagues.

The collaboration wishes to thank Y. Andres, D. Cozza, A. Gandi, R. Puntaferro, T. Scognetti, R. Veenhof for their appreciated contributions during the different phases of the project.

We are also indebted to the CERN test-beam staff, L. Durieu and P. Grafstroem and our administrative staff, S. Barras and S. Stappers. The constant support of B. Ghidini and F. Posa in Bari and of J. Schukraft at CERN was highly appreciated.

References

[1] F. Piuz et al., Nucl. Instr. and Meth. A 433 (1999) 222.
[2] A. Di Mauro et al., Nucl. Instr. and Meth. A 433 (1999) 190.
[3] ALICE Collaboration, Technical Proposal, CERN/LHCC 95-71.
[4] J. Séguinot et al., Nucl. Instr. and Meth. A 297 (1990) 133 and references therein.
[5] Detector R&D Proposal- P35, CERN/DRDC 92-3, CERN/DRDC 92-16 and RD-26 Status Reports CERN/DRDC 93-36, 94-49, 96-20.
[6] HADES, Proposal for a High Acceptance Di-Electrons Spectrometer, GSI, Darmstadt, 1993.
[7] K. Zeitelhack et al., Nucl. Instr. and Meth. A 433 (1999) 201.
[8] COMPASS Proposal, CERN/SPSLC 96-14.
[9] S. Dalla Torre et al., Nucl. Instr. and Meth. A 433 (1999) 207.
[10] ALICE Collaboration, Technical Design Report of the High Momentum Particle Identifier Detector, CERN/LHCC 98-19.
[11] Rob Veenhof, private communication of GARFIELD calculations.
[12] J. Séguinot, Les compteurs Cherenkov: applications et limites pour l'identification des particules. Developpements et perspectives, Ecole J. Curie de Physique Nucleaire, Mabuisson, France, September 1988.
[13] A. Breskin et al., Nucl. Instr. Meth. A 367 (1995) 342.
[14] A. Di Mauro et al., Nucl. Instr. Meth. A 371 (1996) 137.
[15] C.W. Fabjan et al., Nucl. Instr. Meth. A 367 (1995) 240.
[16] M. Spegel, Nucl. Instr. and Meth. A 433 (1999) 366.